

Influence of Vertical Shear of Basic Tangential Wind on the Development and Maintenance of Typhoon

TAO Jianjun* (陶建军), WANG Fang (王芳), LI Chaokui (李朝奎), and HU Xianghui (胡向辉)

Department of Geography, Hunan University of Science and Technology, Xiangtan 411201

(Received August 7, 2012; in final form December 21, 2012)

ABSTRACT

By using a linear symmetric Conditional Instability of Second Kind (CISK) model containing basic flow, we study the interactions between basic flow and mesoscale disturbances in typhoon. The result shows that in the early stage of typhoon formation, the combined action of vertical shear of basic flow at low level and CISK impels the disturbances to grow rapidly and to move toward the center of typhoon. The development of disturbances, likewise, influences on typhoon's development and structure. Analysis of the mesoscale disturbances' development and propagation indicates that the maximum wind region moves toward the center, wind velocity increases, and circulation features of an eye appear. Similarly, when a typhoon decays, the increase of low-level vertical wind shear facilitates the development of mesoscale disturbances. In turn, these mesoscale disturbances will provide typhoon with energy and make the typhoon intensify again. Therefore, it can be said that typhoon has the renewable or self-repair function.

Key words: typhoon, mesoscale disturbances, Conditional Instability of Second Kind, vertical shear

Citation: Tao Jianjun, Wang Fang, Li Chaokui, et al., 2013: Influence of vertical shear of basic tangential wind on the development and maintenance of typhoon. *Acta Meteor. Sinica*, **27**(2), 273–281, doi: 10.1007/s13351-013-0211-y.

1. Introduction

The structural characteristic of the typhoon is one of the important factors affecting its development and movement. Recent researches on the typhoon structure have made new progress (Ding and Li, 2011; Cheng et al., 2011; Li et al., 2009, 2010; Wang et al., 2011). Horizontally, the typhoon has a symmetric or asymmetric structure (Reasor and Montgomery, 2000; Shea and Gray, 1973). The asymmetric structure outside the cloud wall comprises of mesoscale systems such as the spiral cloud bands (Chen and Yau, 2003). How is the relationship between these mesoscale systems and the basic flow of the typhoon? Willoughby (1978) studied the mechanism of spiral rainband in typhoon and pointed out that during the life of typhoon, new mesoscale systems are constantly generated and old ones disappear, and air mass is continually entrained into the center of typhoon, providing energy and angular velocity for the vortex. Chen et

al. (2002) pointed out that landfalling typhoons often form mesoscale vortex at their periphery because of the terrain or environmental convergence effect. These vortices interact with typhoon and are inhaled to core area, leading to typhoon's vorticity increasing and its sustaining on land. Recently, Tao and Xu (2012) studied development and movement of mesoscale disturbances in a tropical weak vortex and found that low-layer vertical wind shear of the vortex can make turbulence spread to the typhoon center, and impels typhoon's formation. Li et al. (2009) once pointed out that when internal rainbands are involved to the typhoon center and gradually form continuous annular convective zone, the diameter of the typhoon eye decreases with the typhoon strengthening. Liu et al. (1999) studied Hurricane Andrew (1992) and found that the radius of maximum wind velocity shrank as the velocity increased. Later, Corbosiero et al. (2005) studied the structure and evolution of Hurricane Elena (1985) and also showed that disturbances move to the

Supported by the National Natural Science Foundation of China (41075046).

*Corresponding author: tao043@163.com.

©The Chinese Meteorological Society and Springer-Verlag Berlin Heidelberg 2013

center. However, whether or not there is a necessary connection between strengthening of these mesoscale systems and the moving of maximum wind velocity in the typhoon is still not very clear, and is worthy of further study.

In view of the above problems, according to the actual structure of tropical cyclone and typhoon, this article studies the effect of vertical wind shear in typhoon on the development and spreading of the mesoscale disturbances and the role of these disturbances in the further development and maintenance of typhoon. It is found that when the tangential wind of typhoon in the low troposphere exhibits an obvious vertical shear, accompanied by condensational heating, mesoscale disturbances will develop rapidly and spread to the typhoon center, providing energy for the typhoon, and the maximum wind velocity moves toward the typhoon center as well, producing an enhanced circulation structure of typhoon center.

2. Kinetic equation

Considering an approximate ringlike or semi-ring disturbance (supposing that its radial scale is much smaller than its tangential scale, e.g., Fig. 6), a symmetric (Willoughby et al., 1984) and linear model of the disturbance in cylindrical coordinates is as follows:

$$\frac{\partial v_\theta^*}{\partial t} + \left(f^* + \frac{\bar{V}_\theta}{r^*} + \frac{\partial \bar{V}_\theta}{\partial r^*} \right) v_r^* + w^* \frac{\partial \bar{V}_\theta}{\partial z} = 0, \quad (1)$$

$$-\left(f^* + \frac{2\bar{V}_\theta}{r^*} \right) v_\theta^* = -\frac{\partial p^*}{\partial r^*}, \quad (2)$$

$$-\theta_e^* = -\frac{\partial p^*}{\partial z^*}, \quad (3)$$

$$\frac{\partial \theta_e^*}{\partial t} + v_r^* \frac{\partial \bar{\theta}_e}{\partial r^*} + \hat{N}^2 w^* = \frac{\bar{\theta}_e}{\bar{T} c_p} Q, \quad (4)$$

$$\frac{\partial(r^* v_r^*)}{r^* \partial r^*} + \frac{\partial w^*}{\partial z^*} = 0. \quad (5)$$

Together with $(v_\theta^*, v_r^*, w^*, \theta_e^*) \equiv \bar{\rho}(v'_\theta, v'_r, w', \frac{g}{\theta'_e} \theta'_e)$

and $\hat{N}^2 = \frac{g}{\bar{\theta}_e} \frac{\partial \bar{\theta}_e}{\partial z}$, the basic state meets

$$f\bar{V}_\theta + \frac{\bar{V}_\theta^2}{r^*} = \frac{1}{\bar{\rho}} \frac{\partial \bar{p}}{\partial r^*}, \quad (6a)$$

$$g = -\frac{1}{\bar{\rho}} \frac{\partial \bar{p}}{\partial z^*}, \quad (6b)$$

$$\left(f + 2 \frac{\bar{V}_\theta}{r^*} \right) \frac{\partial \bar{V}_\theta}{\partial z^*} = \frac{g}{\bar{\theta}_{se}} \frac{\partial \bar{\theta}_{se}}{\partial r^*}, \quad (6c)$$

where θ_e^* is equivalent potential temperature, c_p is specific heat at constant pressure, \bar{T} is average temperature, and Q is the non-adiabatic heating. All others are commonly adopted meteorological symbols, and asterisk denotes dimensional quantity.

The upper atmosphere extends till $w^* = 0$, and the lower boundary is defined on top of the Ekman layer. At the vortex center, $v_r^* = v_\theta^* = 0$. We take $(v_r^*, v_\theta^*) = \bar{V}_0(v_r, v_\theta)$, $r^* = r_0 r$, $t = (\bar{V}_0/r_0)t^*$, $z^* = D_0 z$, $w^* = (\bar{V}_0 D_0/r_0)w$, $\theta_e^* = \frac{\bar{V}_0^2}{D_0} \theta_e$, $\bar{V}_\theta = \bar{V}_0 \bar{V}$, $f = f^* \frac{r_0}{\bar{V}_0}$, and $N^2 = \frac{g}{\bar{\theta}_e} \frac{\partial \bar{\theta}_e}{\partial z} = D_0 \hat{N}^2$. Here r_0 is vortex characteristic radius, \bar{V}_0 is the tangential velocity at the characteristic radius, and D_0 is the vertical scale. Then, the non-dimensional Eqs. (1)–(6) (Tao and Xu, 2012) are given by

$$\frac{\partial v_\theta}{\partial t} + \bar{\zeta} v_r + w \frac{\partial \bar{V}_\theta}{\partial z} = 0, \quad (7)$$

$$-\bar{f} v_\theta = -\frac{\partial p}{\partial r}, \quad (8)$$

$$\frac{\partial}{\partial t} \frac{\partial p}{\partial z} + v_r \frac{\partial \bar{\theta}_e}{\partial r} + S w = \frac{\bar{\theta}_e}{\bar{T} c_p} Q, \quad (9)$$

$$\frac{\partial(r v_r)}{r \partial r} + \frac{\partial w}{\partial z} = 0. \quad (10)$$

Here, $S = \frac{D_0^2}{\bar{V}_0^2} \hat{N}^2 = F^{-1} N^2$ is equivalent to Richard-

son number, $F = \bar{V}_0^2/D_0$ is vorticity disturbance, $\bar{\zeta} = f + \frac{\bar{V}_\theta}{r} + \frac{\partial \bar{V}_\theta}{\partial r}$ is basic vorticity, and $\bar{f} = f + \frac{2\bar{V}_\theta}{r}$.

The basic flow profile adopts the forms discussed by Lei and Chen (2005) and Macafee and Garry (2006). Here, two models are selected.

Miller model:

$$V = \begin{cases} V_m \left(\frac{r}{r_{\max}} \right), & 0 < r < r_{\max} \\ V_m \left(\frac{r_{\max}}{r} \right)^\eta, & r \geq r_{\max} > 0 \end{cases}, \quad (11)$$

DeMaria model:

$$V = V_m \left(\frac{r}{r_{\max}} \right) \exp \left\{ \frac{1}{B} \left[1 - \left(\frac{r}{r_{\max}} \right)^B \right] \right\}, \quad (12)$$

$$0 < r < \infty.$$

Equation (11) is used to discuss the stability and disseminating of the disturbance outside the maximum wind velocity while Eq. (12) is used to simulate disturbances in typhoon. V_m is non-dimensional maximum wind velocity, and r_{\max} and r both are non-dimensional quantities.

By Eq. (10), we obtain the stream function $rv_r = \frac{\partial\psi}{\partial z}$ and $rw = -\frac{\partial\psi}{\partial r}$, and

$$\frac{\partial v_\theta}{\partial t} + \bar{\zeta}_1 \frac{1}{r} \frac{\partial\psi}{\partial z} - \frac{\partial\bar{V}}{\partial z} \frac{1}{r} \frac{\partial\psi}{\partial r} = 0, \quad (13)$$

$$(fr + 2\bar{V})v_\theta = r \frac{\partial p}{\partial r}, \quad (14)$$

$$\frac{\partial^2 p}{\partial t \partial z} + \frac{\partial\bar{\theta}_e}{\partial r} \frac{1}{r} \frac{\partial\psi}{\partial z} - S \frac{1}{r} \frac{\partial\psi}{\partial r} = \frac{\bar{\theta}_e}{\bar{T}c_p} Q. \quad (15)$$

For simplicity, we use a two-layer model. The CISK parameterization of heating is expressed as

$$Q = \frac{\mu L}{2\Delta} (\bar{q}_{s3} - \bar{q}_{s1}) \left(w_2^* + \frac{1}{2} w_e^* \right), \quad (16)$$

$$w_e^* = \frac{1}{2} h_E^* \left(\frac{\partial v_{\theta e}^*}{\partial r} + \frac{v_{\theta e}^*}{r} \right). \quad (17)$$

Moreover, we assume that maximum wind speed occurs at the top of the friction layer (Li et al., 1985). By substituting non-dimensionalized Eqs. (16)–(17) into Eqs. (13)–(15), we obtain

$$\frac{\partial v_{\theta 1}}{\partial t} + \bar{\zeta}_1 \frac{1}{r} \frac{\psi_2 - \psi_e}{\Delta} - \bar{V}_{z1} \frac{1}{r} \frac{\partial\psi_1}{\partial r} = 0, \quad (18)$$

$$\frac{\partial v_{\theta 3}}{\partial t} - \bar{\zeta}_3 \frac{1}{r} \frac{\psi_2}{\Delta} - \bar{V}_{z3} \frac{1}{r} \frac{\partial\psi_3}{\partial r} = 0, \quad (19)$$

$$\bar{f}_1 v_{\theta 1} = \frac{\partial p_1}{\partial r}, \quad \bar{f}_3 v_{\theta 3} = \frac{\partial p_3}{\partial r}, \quad (20)$$

$$\frac{\partial p_3 - p_1}{\partial t} \frac{1}{\Delta} + \frac{\partial\bar{\theta}_{e2}}{\partial r} \frac{1}{r} \frac{\psi_3 - \psi_1}{\Delta} - (S - h) \frac{1}{r} \frac{\partial\psi_2}{\partial r} = \frac{\mu H}{2} K \left(\frac{\partial v_{\theta 0}}{\partial r} + \frac{v_{\theta 0}}{r} \right). \quad (21)$$

Here, the subscripts 0, 1, 2, and 3 represent the top of Ekman layer, lower troposphere, middle troposphere, and upper troposphere, and $\bar{V}_{z1} = \frac{\bar{V}_2 - \bar{V}_0}{\Delta}$ and $\bar{V}_{z3} = \frac{\bar{V}_4 - \bar{V}_2}{\Delta}$. The other symbols have their standard meteorological meaning.

We approximatively take $\psi_1 = \frac{1}{2}(\psi_2 + \psi_e)$, $\psi_3 = \frac{1}{2}(\psi_2 + \psi_4)$, then $\psi_3 - \psi_1 = -\frac{1}{2}\psi_e$. According to the upper boundary conditions, we assume $\psi_4 = 0$. Sub-

stitute these into Eqs. (18)–(21), they become

$$\frac{\partial v_{\theta 1}}{\partial t} + \bar{\zeta}_1 \frac{1}{r} \frac{\psi_2 - \psi_e}{\Delta} - \bar{V}_{z1} \frac{1}{2r} \frac{\partial(\psi_2 + \psi_e)}{\partial r} = 0, \quad (22)$$

$$\frac{\partial v_{\theta 3}}{\partial t} - \bar{\zeta}_3 \frac{1}{r} \frac{\psi_2}{\Delta} - \bar{V}_{z3} \frac{1}{2r} \frac{\partial\psi_2}{\partial r} = 0, \quad (23)$$

$$\begin{aligned} & \frac{\partial \bar{f}_3 v_{\theta 3} - \bar{f}_1 v_{\theta 1}}{\partial t} \frac{1}{\Delta} - \frac{\partial^2 \bar{\theta}_{e2}}{\partial r^2} \frac{1}{2r} \frac{\psi_e}{\Delta} + \frac{\partial \bar{\theta}_{e2}}{\partial r} \frac{\psi_e}{2\Delta r^2} \\ & - \frac{\partial \bar{\theta}_{e2}}{\partial r} \frac{1}{2\Delta r} \frac{\partial\psi_e}{\partial r} - (S - \mu H) \left(\frac{1}{r} \frac{\partial^2 \psi_2}{\partial r^2} - \frac{1}{r^2} \frac{\partial\psi_2}{\partial r} \right) \\ & = \frac{\mu H}{2} K \left(\frac{\partial^2 v_{\theta 0}}{\partial r^2} - \frac{v_{\theta 0}}{r^2} + \frac{1}{r} \frac{\partial v_{\theta 0}}{\partial r} \right). \end{aligned} \quad (24)$$

Note that the non-dimensional form of Eq. (17) is $\frac{1}{r} \frac{\partial\psi_e}{\partial r} = -K \frac{\partial r v_{\theta e}}{r \partial r}$, which is $\psi_e = -K r v_{\theta 1}$. Equations (22)–(24) will be discussed in this paper; they can be used to study the development and movement of disturbances in typhoon.

3. Disturbance's stability and phase velocity

Using the method by Lu et al. (2004) and Corbosiero et al. (2006), we assume:

$$(v_{\theta 1}, v_{\theta 3}, \psi_2) = (\tilde{v}_{\theta 1}, \tilde{v}_{\theta 3}, \tilde{\psi}_2) e^{ilr + i\sigma t}. \quad (25)$$

Here, $\tilde{v}_{\theta 1}$, $\tilde{v}_{\theta 3}$, and $\tilde{\psi}_2$ are regarded as slowly varying functions, and l is the radial wave number.

Substitute Eq. (25) into Eqs. (22)–(24), we have

$$\begin{aligned} & i\sigma v_{\theta 1} + \bar{\zeta}_1 \frac{1}{r} \frac{\psi_2}{\Delta} + \bar{\zeta}_1 \frac{K v_{\theta 1}}{\Delta} \\ & - \bar{V}_{z1} \frac{1}{2} \left[\frac{il\psi_2}{r} - K \left(\frac{1}{r} + il \right) v_{\theta 1} \right] = 0, \end{aligned} \quad (26)$$

$$i\sigma v_{\theta 3} - \bar{\zeta}_3 \frac{1}{r} \frac{\psi_2}{\Delta} - \bar{V}_{z3} \frac{il\psi_2}{2r} = 0, \quad (27)$$

$$\begin{aligned} & \frac{i\sigma \bar{f}_3 v_{\theta 3} - i\sigma \bar{f}_1 v_{\theta 1}}{\Delta} + K \frac{\partial^2 \bar{\theta}_{e2}}{\partial r^2} \frac{v_{\theta 1}}{2\Delta} - K \frac{\partial \bar{\theta}_{e2}}{\partial r} \frac{v_{\theta 1}}{2\Delta r} \\ & + K \frac{\partial \bar{\theta}_{e2}}{\partial r} \frac{il v_{\theta 1}}{2\Delta} - (S - \mu H) \left(-\frac{l^2}{r} - \frac{il}{r^2} \right) \psi_2 = \\ & \frac{\mu H}{2} K \left(-l^2 - \frac{1}{r^2} + \frac{il}{r} \right) v_{\theta 1}. \end{aligned} \quad (28)$$

The frequency equation is obtained from Eqs. (26)–(28) as

$$i\sigma(\alpha_1 + \alpha_2) + \beta = 0. \quad (29)$$

Here,

$$\begin{aligned} \alpha_1 &= (S_2 - \mu H) \left(l^2 + \frac{il}{r} \right), \\ \alpha_2 &= \left(\frac{\bar{\zeta}_3}{r\Delta} + \frac{iV_{z3}}{2r} \right) \frac{\bar{f}_3}{\Delta} + \left(\frac{\bar{\zeta}_1}{r\Delta} - \frac{i\bar{V}_{z1}}{2r} \right) \frac{\bar{f}_1}{\Delta}, \\ \beta &= \left(\frac{\bar{\zeta}_1 K}{\Delta} + \frac{KV_{z1}}{2} \left(il + \frac{1}{r} \right) \right) (S_2 - \mu H) \\ &\quad \cdot \left(\frac{l^2}{r} + \frac{il}{r^2} \right) + \left(\frac{\bar{\zeta}_3}{r\Delta} + \frac{i\bar{V}_{z3}}{2r} \right) \left[\frac{\bar{\zeta}_1 K}{\Delta} \right. \\ &\quad \left. + \frac{K\bar{V}_{z1}}{2} \left(\frac{1}{r} + il \right) \right] \frac{\bar{f}_3}{\Delta} - \left[\frac{K}{\Delta} \left(\frac{\partial^2 \bar{\theta}_{e2}}{2\partial r^2} \right. \right. \\ &\quad \left. \left. - \frac{1}{2r} \frac{\partial \bar{\theta}_{e2}}{\partial r} + il \frac{\partial \bar{\theta}_{e2}}{2\partial r} \right) + \frac{\mu HK}{2} \left(-\frac{il}{r} \right. \right. \\ &\quad \left. \left. + l^2 + \frac{1}{r^2} \right) \right] \left(\frac{\bar{\zeta}_1}{r\Delta} - \frac{i\bar{V}_{z1}}{2r} \right). \end{aligned} \quad (30)$$

Firstly, substituting the Miller model Eq. (11) into Eq. (30), we study the stability and phase velocity in the region outside maximum wind velocity, where desirable parameters are $r_0 = 100$ km, $D_0 = 10$ km, $\Delta = 0.45$, $H = 1.1$, $\lambda = 1$, $f^* = 0.370 \times 10^{-4} \text{ s}^{-1}$, $\bar{N}^2 = 10^{-4} \text{ s}^{-1}$, $\bar{V}_0 = 100 \text{ m s}^{-1}$.

From Fig. 1, we can see that the vertical shear of basic flow has a great influence on stability. For instance, when we take $V_0 = 0.35$ and $V_2 = 0 \text{ m s}^{-1}$, the growth rate is $1.8 \times 10^{-5} \text{ s}^{-1}$; when we take $V_0 = 0.35 \text{ m s}^{-1}$ and $V_2 = 0.35$ (namely vertical shear is zero), the growth rate is only $0.4 \times 10^{-5} \text{ s}^{-1}$. This result is consistent with that of a rigid base flow (Tao and Xu, 2012). In addition, it can be seen from Fig. 1 that the disturbance's growth rate and phase velocity are correlated with wave number. Specifically, when wave number is larger than 3 (the dimensional wavelength is 100–200 km), both the growth rate and negative phase velocity are bigger, so the vertical shear is advantageous to development of the mesoscale system. Of course, if the disturbance's radial scale is too small, it is difficult to form a successive and lager-scale ringlike structure, the influence of vertical wind shear on typhoon structure would be relatively smaller.

Ding et al. (1986) studied a typhoon (1975) and found that in the early stages of typhoon development, the maximum wind velocity is at 900–850 hPa; when it attains maturity, relatively homogeneous strong wind spreads from 850 to 500 hPa, and the vertical shear

is reduced at once. That is to say, the mature typhoon's vertical shear is smaller at low levels. Conversely, early-stage or weakened typhoon's low-level vertical shear is larger, so it is conducive to the disturbance development. Vertical shear also helps to result in a high asymmetry structure of typhoon (Frank and Ritchie, 2001).

In addition, the phase velocity of disturbance is negative, suggesting that the disturbance will propagate toward the typhoon center, and the greater the vertical shear is, the faster the disturbance moves. Note this model filters out gravity waves and retains only CISK wave. As mentioned above, the mature typhoon's vertical shear is smaller, the disturbance's spread velocity toward center is very slow; whereas in early-stage typhoon and decayed typhoon, the vertical shear is greater, so the disturbance's spread velocity toward center is faster, which feeds back more energy to typhoon. This may cause the typhoon to be re-strengthened. It can be said that typhoon may have a "self-healing" ability to make itself maintain a longer time.

From Fig. 2, we can see that the growth rate is larger near the maximum wind velocity center than away from the center because of distribution of basic flow (see Eq. (11)); meanwhile, the phase velocity also changes with the radius, so when a disturbance moves toward the center, it will get deformed. In addition,

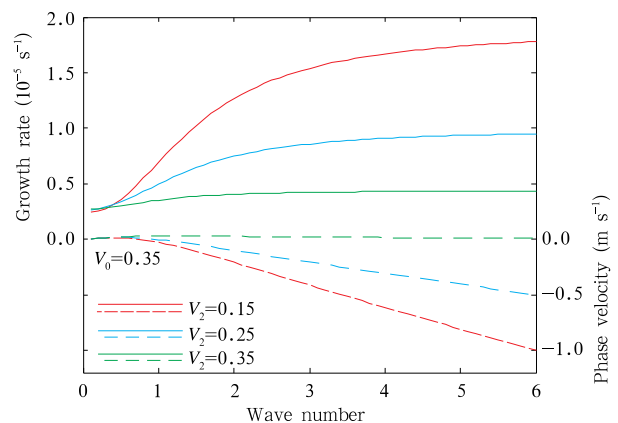


Fig. 1. Variations of the growth rate (solid lines) and phase velocity (dashed lines) with wave number under different tangential wind shear conditions ($\eta = 0.5$, $V_4 = 0 \text{ m s}^{-1}$, $\mu = 0.8$, $r = 200 \text{ km}$).

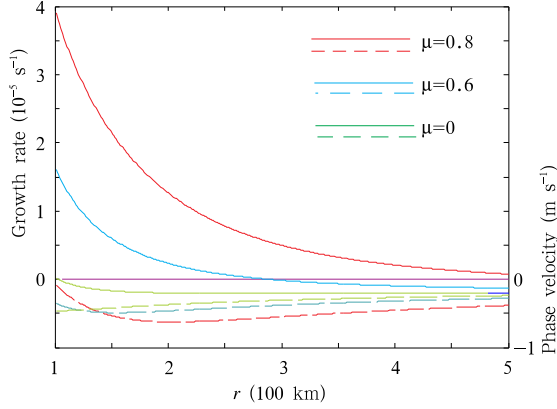


Fig. 2. Variations of the growth rate (solid lines) and phase velocity (dashed lines) with distance from the typhoon center under different condensational heating conditions ($l = 2$, $V_0 = 0.35 \text{ m s}^{-1}$, $V_2 = 0.15 \text{ m s}^{-1}$, $r_{\text{max}} = 1$, and $\eta = 0.5$).

the growth rate and propagation velocity are also related to condensational heating and they are the result of combined action of vertical shear and CISK.

4. Physical mechanism

Figure 3 shows the physical mechanism of disturbance development and propagation under the vertical shear condition. In Fig. 3, because tangential wind in low layer is larger than in higher layer, the vertical advection effect makes the tangential wind in the “A” (positive vorticity) region increase; conversely, the tangential wind in the “B” (negative vorticity) region decreases. Because $\zeta \propto \frac{v_\theta}{r}$, vorticity is increased in “A” region and decreased in “B” region. Coupled with the effect of condensational heating, the disturbances grow faster. Meanwhile, the tangential velocity in “A” region is increased and the velocity in “B” region decreased, and because $\zeta \propto \frac{\partial v_\theta}{\partial r}$, the vorticity increases between “A” and “B”; thus, the disturbances propagate inwards.

5. Disturbance evolution

Because the frequency equation contains radius r , the above conclusion is only suitable for initial disturbance. With the increase of time, disturbance amplitude will change. To further verify the conclusions from the above qualitative analysis, we must study the

time evolution of the disturbances.

We will use numerical method to solve Eqs. (22)–(24). They are written in the following form

$$\frac{\partial v_{\theta 1}}{\partial t} + \bar{\zeta}_1 \frac{1}{r} \frac{\psi_2 - \psi_e}{\Delta} - \bar{V}_{z1} \frac{1}{2r} \frac{\partial(\psi_2 + \psi_e)}{\partial r} = 0, \quad (31)$$

$$\frac{\partial v_{\theta 3}}{\partial t} - \bar{\zeta}_3 \frac{1}{r} \frac{\psi_2}{\Delta} - \bar{V}_{z3} \frac{1}{2r} \frac{\partial \psi_2}{\partial r} = 0, \quad (32)$$

$$\begin{aligned} & -(S_2 - \mu H) \Delta \frac{\partial^2 \psi_2}{\partial r^2} + \left(\frac{\bar{V}_{z3} \bar{f}_3}{2} - \frac{\bar{V}_{z1} \bar{f}_1}{2} \right. \\ & \left. + \frac{(S_2 - \mu H) \Delta}{r} \right) \frac{\partial \psi_2}{\partial r} + \left(\frac{\bar{\zeta}_1 \bar{f}_1}{\Delta} + \frac{\bar{\zeta}_3 \bar{f}_3}{\Delta} \right) \psi_2 = \\ & \bar{\zeta}_1 \bar{f}_1 \frac{\psi_e}{\Delta} + \bar{V}_{z1} \frac{\bar{f}_1}{2} \frac{\partial \psi_e}{\partial r} + \frac{\partial^2 \bar{\theta}_{e2}}{\partial r^2} \frac{\psi_e}{2} - \frac{\partial \bar{\theta}_{e2}}{\partial r} \frac{\psi_e}{2r} \\ & + \frac{\partial \bar{\theta}_{e2}}{\partial r} \frac{1}{2} \frac{\partial \psi_e}{\partial r} - \frac{\mu H \Delta}{2} \left(\frac{\partial^2 \psi_e}{\partial r^2} - \frac{1}{r} \frac{\partial \psi_e}{\partial r} \right). \end{aligned} \quad (33)$$

First, we solve Eqs. (31)–(32) to obtain values of $v_{\theta 1}$ and $v_{\theta 3}$ under initial condition, then substitute them into Eq. (33) to obtain value of ψ_2 using chasing method. We set the model with a 1-km grid spacing and use the boundary conditions $v_r = v_\theta = 0$ at $r = 0$.

Because condensational heating occurs mainly in the region with convergence in the boundary layer, in the process of calculation, if w_e is less than zero, we let μ equal zero.

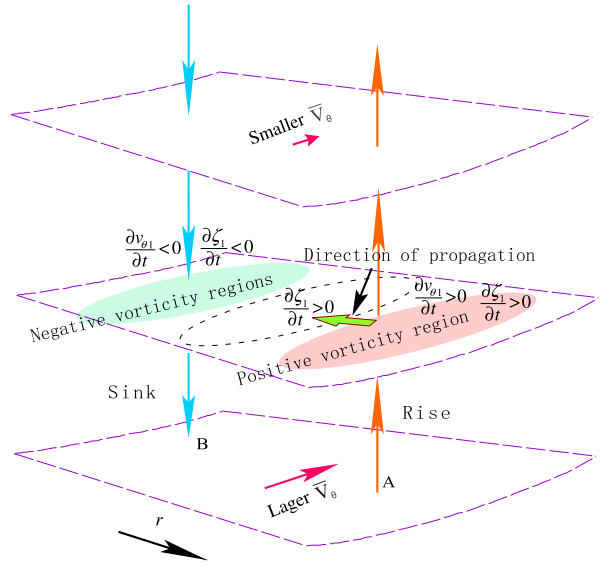


Fig. 3. Schematic diagram of physical mechanism of the disturbance development and propagation under certain condition of vertical shear of basic flow.

Using the above model, we first study the formation of typhoon with the basic flow given by Eq. (12). We take $B = 1.6$ and $r_{\max} = 1.8$, namely, its maximum value is at the distance of 180 km to the center (see Fig. 4). The initial disturbance is also shown in Fig. 4. Its maximum value is at the distance of about 220 km to the center.

Figure 4 shows the change of disturbance in different vertical shears of basic flow after 30 h. When the vertical shear is larger (e.g., $V_0 = 0.25$ and $V_2 = 0.1 \text{ m s}^{-1}$), the disturbance grows very fast and the maximum wind velocity is up to 44 m s^{-1} . When the vertical shear is smaller, e.g., $V_0 = 0.25$ and $V_2 = 0.2 \text{ m s}^{-1}$, the maximum wind velocity is only about 13 m s^{-1} .

Figure 4 also shows that the disturbance's moving velocity and the basic flow's vertical shear are closely related. The larger the vertical shear is, the faster the disturbance moves. For instance, when we take $V_0 = 0.25$ and $V_2 = 0.1 \text{ m s}^{-1}$, the maximum velocity region of disturbance is at a distance of 180 km away from its initial position after 30 h; when we take $V_0 = 0.25$ and $V_2 = 0.2 \text{ m s}^{-1}$, the maximum value of disturbance is at a distance of only about 60 km away from its initial position, i.e., its movement speed is smaller.

Figure 5 corresponds to a tropical cyclone case with initial disturbance bearing weak tangential wind (maximum value is 3 m s^{-1}). It is an example that shows various components of the disturbance changing and moving. When the disturbance develops, it moves toward the tropical cyclone center.

Figure 5a shows change of the disturbance's tangential wind. Near the vortex center, the tangential wind is negative and rotates clockwise, which partly offsets the positive rotating basic flow, so the wind velocity will become very small near the center (Fig. 5d); by then, features of a tropical cyclone eye appear.

Figures 5b and 5c show radial velocity and vertical movement of the disturbance. From Fig. 5c, we can see when the disturbance moves near the center, sinking movement over the center appears; outside it, upward movement appears. These are the circulation characteristics near the center of the typhoon. Here, the vertical and radial movements are very sim-

ilar with works of Liu et al. (1999).

Figure 5d reflects the process during which the maximum tangential wind increases gradually and moves toward the center.

Of course, this model is too simple. The actual typhoon is a nonlinear system, and this model can only explain some phenomena qualitatively.

6. Example analysis

In order to verify the above theoretical results, we use NCEP data to analyze the development process of some typhoon cases. Generally speaking, vertical shear of basic flow is larger in initial-stage typhoons than in mature typhoons.

Figure 6 shows the formation process of Typhoon Nanmadol (2011). From Figs. 6a and 6b, we can see that, in the early stage, the vertical wind shear is bigger and its range is wider in the lower troposphere, and it has an obvious tangential component (but the vertical shears are not the same in different directions, consistent with Kepert (2006)). At this time, a disturbance develops fast and gradually evolves into a ring-like maximum wind band while moving toward the typhoon center. However, with the development of the system, the range and strength of the vertical wind shear clearly become smaller (Fig. 6c), the maximum wind velocity band no longer moves toward the center;

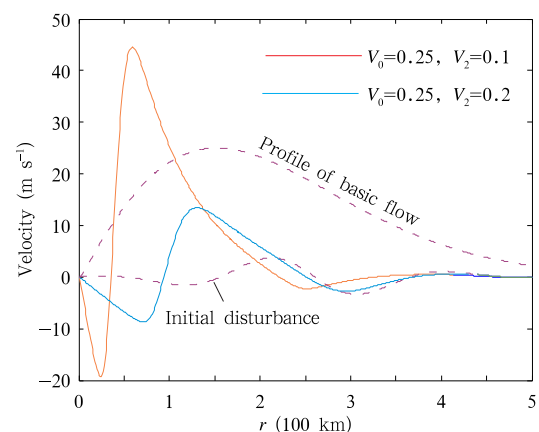


Fig. 4. Change of disturbance velocity with different vertical shears of basic flow $\mu = 0.8$ and $V_4 = 0$. Dashed lines give the base flow and initial disturbance profiles. Solid lines give profiles of the disturbance after 30 h.

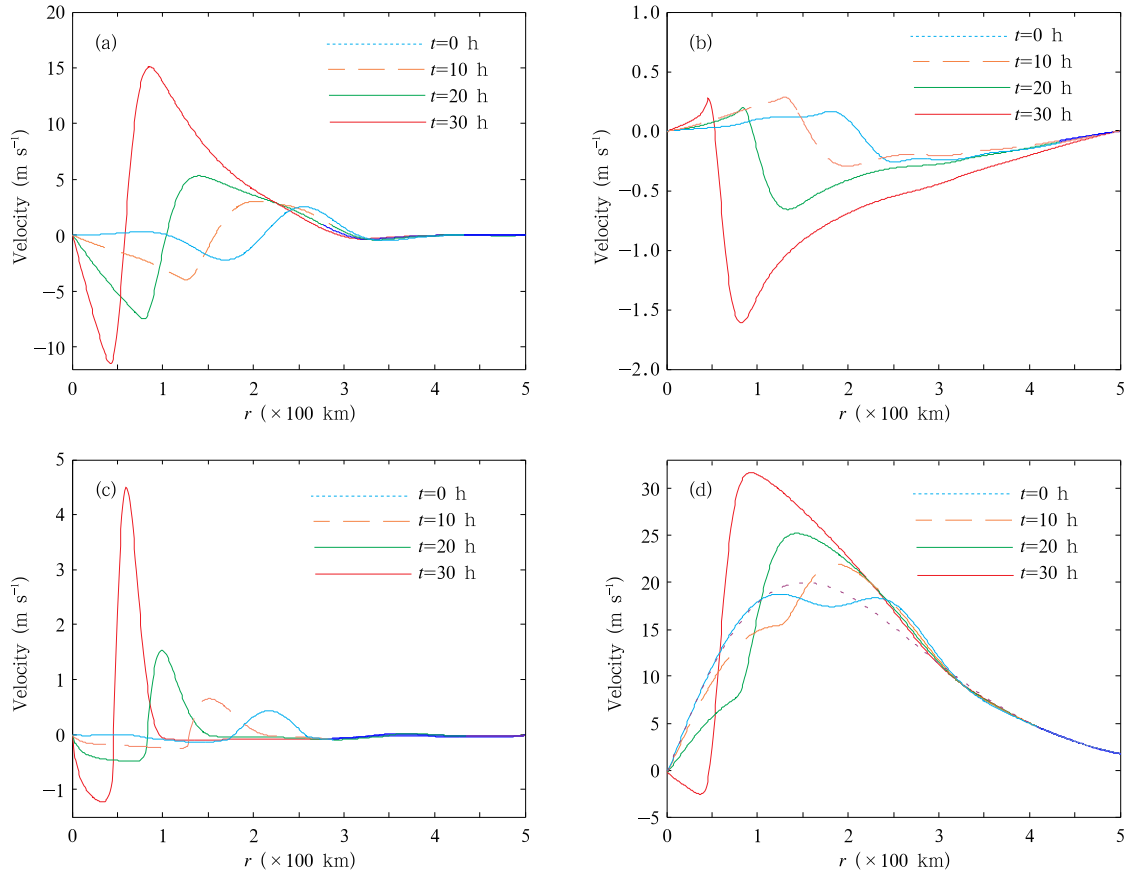


Fig. 5. Growing and moving processes of the disturbance ($V_0 = 20 \text{ m s}^{-1}$, $V_2 = 5 \text{ m s}^{-1}$, $V_4 = 0 \text{ m s}^{-1}$). (a) $v_{\theta 1}$, (b) v_{r1} , (c) w_2 , and (d) $v_{\theta 1} + V_0$. Dashed line in (d) denotes the profile of base flow. Other parameter values are the same as in the text.

instead, it forms the structure of a tropical cyclone eye in the mature stage. These are consistent with theoretical analysis results.

7. Summary

The structure and intensity change of the typhoon is an important aspect of typhoon forecasting. However, the related physical mechanisms are still not very clear. The instability of base flow can stimulate the mesoscale waves in typhoon (Tao and Li, 2009), causing energy consumption. Conversely, typhoon also needs the mesoscale system to feed it energy. Then, how the typhoon and mesoscale system interact is still worthy of further study.

By using a linear, symmetric CISK model includ-

ing the basic flow, this study focuses on the interaction between basic flow of typhoon and mesoscale disturbances. The results may have some significance for explaining the formation and structural change of typhoons. During the early stage of typhoon formation, mesoscale disturbances follow the maximum wind region to move toward the typhoon center till wind velocity increases and circulation features of a tropical cyclone eye appear. When a typhoon decays, the increasing of vertical shear at low level will be good for development of mesoscale disturbances. In turn, these disturbances provide typhoon with energy and make the typhoon strengthen again. Therefore, we can say that typhoon has a renewable or self-repair function.

Because the model used is too simple, we just do some qualitative analysis. In order to know more

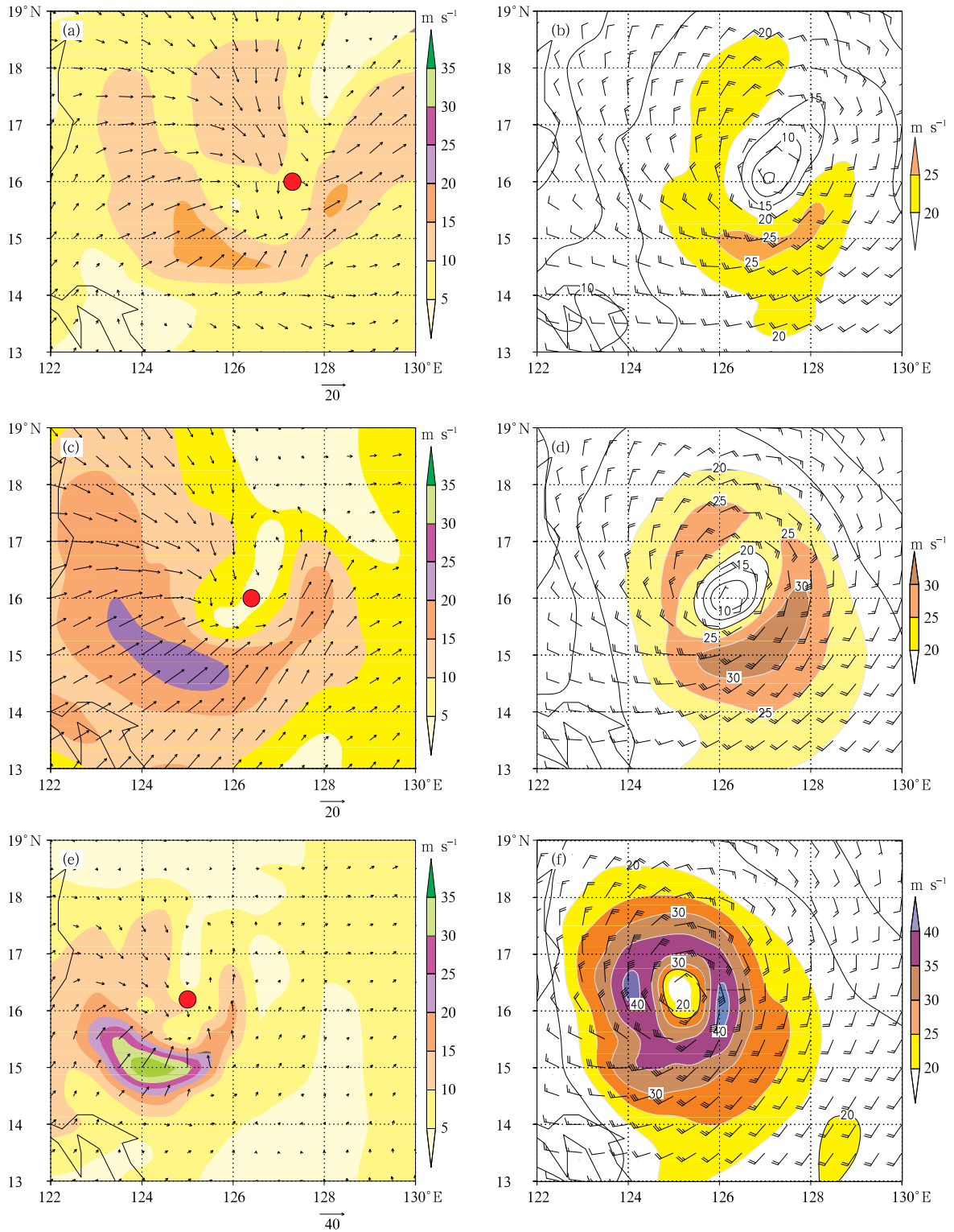


Fig. 6. Evolution of vertical shear (left panels) and wind field (right panels) in Typhoon Nanmadol (2011). Left panels denote the vector $\mathbf{v}_{900\text{hPa}} - \mathbf{v}_{500\text{hPa}}$, and the shadings reflect the strength of the vertical wind shear. Right panels denote the wind field at 900 hPa, in which shadings reflect the area of high winds at 900 hPa.

about the typhoon's real change, we must use more complex nonlinear models.

Acknowledgments. The authors would like to thank the anonymous reviewers and editors for providing valuable comments.

REFERENCES

- Chen Lianshou, Xu Xiangde, and Luo Zhexian, 2002: *Introduction of Tropical Cyclone Dynamics*. China Meteorological Press, Beijing, 317–318. (in Chinese)
- Chen Yongsheng and M. K. Yau, 2003: Asymmetric structures in a simulated landfalling hurricane. *J. Atmos. Sci.*, **60**, 2294–2312.
- Cheng Rui, Yu Rucong, Fu Yunfei, et al., 2011: Impact of cloud microphysical processes on the simulation of Typhoon Rananim near shore. Part I: Cloud structure and precipitation features. *Acta Meteor. Sinica*, **25**(4), 441–455.
- Corbosiero, K. L., M. John, and M. L. Black, 2005: The structure and evolution of Hurricane Elena (1985). Part I: Symmetric intensification. *Mon. Wea. Rev.*, **133**, 2905–2920.
- , —, R. A. Anantha, et al., 2006: The structure and evolution of Hurricane Elena (1985). Part II: Convective asymmetries and evidence for vortex Rossby waves. *Mon. Wea. Rev.*, **134**, 3074–3091.
- Ding Deping and Li Ying, 2011: A study on typhoon-induced rainfalls over Beijing: Statistics and case analysis. *Acta Meteor. Sinica*, **25**(6), 742–753.
- Ding Yihui, Zhang Jian, and Liu Yuezheng, 1986: Further analysis of Typhoon (197501)'s structure and dynamics. *Acta Oceanologica Sinica*, **8**(1), 21–30.
- Frank, W. M., and E. A. Ritchie, 2001: Effects of vertical wind shear on the intensity and structure of numerically simulated hurricanes. *Mon. Wea. Rev.*, **129**, 2249–2268.
- Keper, J. D., 2006: Observed boundary layer wind structure and balance in the hurricane core. Part I: Hurricane Georges. *J. Atmos. Sci.*, **63**, 2169–2193.
- Lei Xiaotu and Chen Lianshou, 2005: A method to construct tropical cyclone wind distribution models and estimate its characteristic parameters. *Chinese J. Geophys.*, **48**(1), 25–31. (in Chinese)
- Li Chongyin, Ye Duzheng, Huang Ronghui, et al., 1985: *Introduction to Dynamic Meteorology*. China Meteorological Press, Beijing, 225–226. (in Chinese)
- Li Ying, Qian Chuanhai, and Chen Lianshou, 2009: A study on the eyewall expansion of Typhoon Sepat (0709) during its landfall process. *Acta Meteor. Sinica*, **67**(5), 799–810. (in Chinese)
- , Chen Lianshou, Qian Chuanhai, et al., 2010: Study on formation and development of a mesoscale convergence line in Typhoon Rananim. *Acta Meteor. Sinica*, **24**(4), 413–425.
- Liu Yubao, Zhang Dalin, and M. K. Yau, 1999: A multi-scale numerical study of Hurricane Andrew (1992). Part II: Kinematics and inner-core structures. *Mon. Wea. Rev.*, **127**, 2597–2615.
- Lu Hancheng, Kang Jianwei, Kou Zheng, et al., 2004: Dynamics features of the mesoscale mixed wave in the typhoon. *Natural Sciences Progress*, **14**, 541–547. (in Chinese)
- Macafee, A. W., and M. P. Garry, 2006: Development and testing of tropical cyclone parametric wind models tailored for midlatitude application—preliminary results. *J. Appl. Meteor. Climatol.*, **45**, 1244–1260.
- Reasor, P. D., and M. T. Montgomery, 2000: Low-wavenumber structure and evolution of the hurricane inner core observed by airborne dual-doppler radar. *Mon. Wea. Rev.*, **128**, 1653–1680.
- Shea, D. J., and W. M. Gray, 1973: The hurricane's inner core region. Part I: Symmetric and asymmetric structure. *J. Atmos. Sci.*, **30**, 1544–1564.
- Tao Jianjun and Li Chaokui, 2009: The formation mechanism and evolution of the double spiral arms in vortex. *Acta Phy. Sinica*, **58**, 4313–4319. (in Chinese)
- and Xu Xianghui, 2012: The development and dissemination characteristic of disturbances in weak tropical cyclones. *Acta Phy. Sinica*, **61**(16), 129202.2-129202.7. (in Chinese)
- Wang Mingjun, Zhao Kun, and Wu Dan, 2011: The T-TREC technique for retrieving the winds of land-falling typhoons in China. *Acta Meteor. Sinica*, **25**(1), 91–103.
- Willoughby, H. E., 1978: The vertical structure of hurricane rainbands and their interaction with the mean vortex. *J. Atmos. Sci.*, **35**, 849–858.
- , H. L. Jin, S. J. Lord, et al., 1984: Hurricane structure and evolution as simulated by an axisymmetric nonhydrostatic numerical model. *J. Atmos. Sci.*, **41**, 1170–1186.